An Investigation of the Near-Field Wake behind a Full-Scale Test Aircraft

Lawrence J. Mertaugh* and Rustom B. Damania†
Mississippi State University, Mississippi State, Miss.
and
Frederick L. Paillet‡
Air Force Flight Dynamics Laboratory, Wright-Patterson Air Force Base, Ohio

Three-dimensional velocity field measurements were made on three transverse measurement planes located at 7.7, 33.3, and 61.2 in. behind the inboard-wing trailing edge of an aircraft in flight. The test aircraft was an L-19 modified to incorporate a distributed suction boundary-layer control system. Test data were obtained at various lift coefficients and with both zero and full flap deflections. Flowfield measurements were made with a total-vector hot-film probe mounted to a boom and traversing mechanism attached to the rear fuselage of the test aircraft. The velocity measurements allowed computation of all three components of vorticity at the 7.7-in. plane and the normal (to the measurement plane) component of vorticity at the other two planes. The test results are presented as a series of contours of the various vorticity component values in the measurement planes. A typical set of axial velocity contours has also been provided. The plotted contours show a reproducible set of features, which are always associated with the formation of a concentrated core of axial vorticity. The test data are also compared to the predictions of a two-dimensional inviscid wake calculation based on measured wing loading for the L-19.

I. Introduction

THE wake turbulence problem has prompted an extensive series of theoretical and experimental investigations of the vorticity field generated by a lifting surface passing through a fluid medium. An introduction to the large amount of literature on this subject can be obtained by consulting the published proceedings of a symposium held in 1970.[1] Theoretical studies have often produced inconclusive results because detailed experimental data with which to compare predictions were lacking. Wake measurements obtained without the uncertainty of scale effects and the artifical constraints associated with most laboratory environments are especially scarce. The most applicable measurements are those obtained from the wake of an aircraft in actual flight. Such measurements have been made with meteorologic towers and wake-penetrating aircraft, but these are situations in which the measurement system must have a profound influence on the velocity field being measured. Full-scale flight tests can therefore provide more directly useful results but pose enormous problems in the acquisition of unbiased test data.

Most of the full-scale flight test data currently available pertain to the far-wake region, as required by the nature of the measuring systems (anemometer towers and penetrating aircraft). These measurements have been correlated with many wake-decay models developed for axisymmetric and quasicylindrical vortices (the term quasicylindrical applies when radial derivatives are much larger than axial derivatives). A much more difficult question is the relation between generator characteristics and the parameters that describe the cylindrical vortex. Theoretical investigators confront this problem when they define the initial conditions for their votex decay calculations. The assumption of a particular set of such conditions often introduces an unsatisfactory amount of empiricism. Wind-tunnel measurements of the velocity field immediately behind lifting surfaces[2] show that a definite structure is associated with the growing vortex core in the near wake and that the core may contain either an axial velocity excess or defect. A comparison between wind-tunnel and in-flight measurements by McCormick et al.[3] demonstrated a surprising amount of disagreement. The McCormick results also indicated that the two vortex filaments remaining in the far wake contain only a fraction of the total vorticity which is available immediately behind the wing trailing edge. Because the initial condition problem is so important for the whole class of vortex decay calculations, one would like to predict how much of the circulation around the lifting surface is ultimately incorporated into the trailing vortex, and how rapidly the wake system attains its far-field character.

The research effort described in this article was an attempt to provide detailed definition of the near wake behind a flight-test aircraft, and to compare this information with a typical two-dimensional inviscid wake rollup calculation. The data presented in the figures are the combined results of two test programs conducted at separate times. This experimental effort is part of a long-term program at Mississippi State University that is intended to provide a better understanding of trailing vortex formation and dissipation. The present results concentrate on vorticity data acquired within one chord length of the wing trailing edge. It is anticipated that methods for attaining comparable measurements at distances further downstream will be devised in the future.

II. Test Equipment

The test data presented in this article were obtained behind the wing of a high-lift L-19 aircraft. The test aircraft is shown in Fig. 1 with the probe support structure mounted in the "mid" position (the measurement stations are defined subsequently). This particular aircraft has been modified to

Received Sept. 21, 1976; revision received May 17, 1977.
Index categories: Aerodynamics; Computational Methods; Jets, Wakes, and Viscid-Inviscid Flow Interactions.

*Department of Aerophysics and Aerospace Engineering; presently Aerospace Engineer with the Naval Air Test Center, Patuxent River, Md.
†Department of Aerophysics and Aerospace Engineering; presently Assistant Professor, Aeronautics Department, Indian Institute of Science, Bangalore, India.
‡Presently Assistant Professor, Geology Department, Wright State University, Dayton, Ohio.

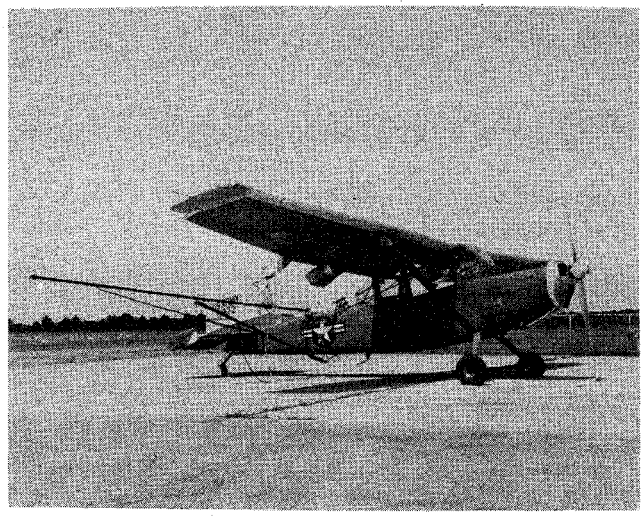

Fig. 1 Test aircraft with the wake measurement boom in the mid position.

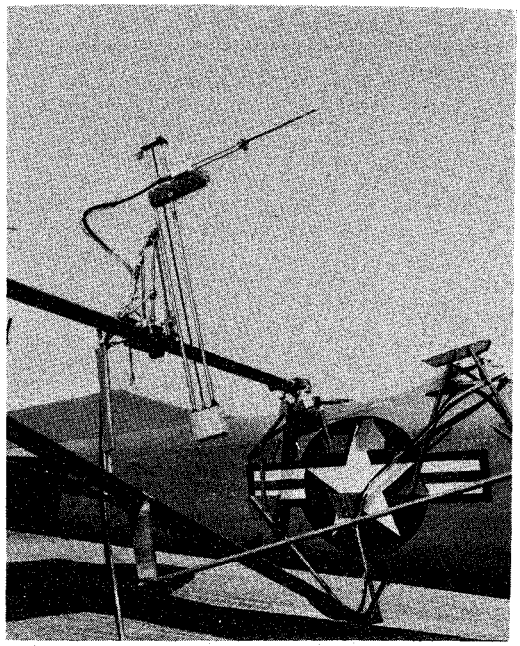

Fig. 2 Probe vertical traversing mechanism in the mid position.

incorporate a distributed suction boundary-layer control (BLC) system. The modifications include an increased wing leading-edge radius, modified wingtips, increased-span plain flaps, increased vertical tail area, and improved streamlining of the aft window area. The distributed suction is accomplished by pumping a portion of the low-energy boundary-layer flow through many rows of small-diameter holes drilled in the upper surface of the wing and flaps. No suction is applied on the aileron or wingtip surfaces. The suction is maintained by two wing-mounted blowers located in fairings under each wing. The blowers are driven by hydraulic motors. The total volume flow of approximately 8000 ft^3/min is pumped by these blowers; peak exit velocity is about 120 fps. The wing geometry for the test aircraft is

$S = 176.8\ ft^2$ (surface area)
$b = 36.00$ ft (wingspan)
$c_R = 5.43$ ft (wingroot chord)
$c_T = 3.58$ ft (wingtip chord)
$c_{ave} = 4.91$ ft (average wing chord)
aspect ratio = 7.33

The average aircraft weight during the flight tests was 2515 lb. Both weight and center of gravity were maintained as close to constant as possible for all test configurations.

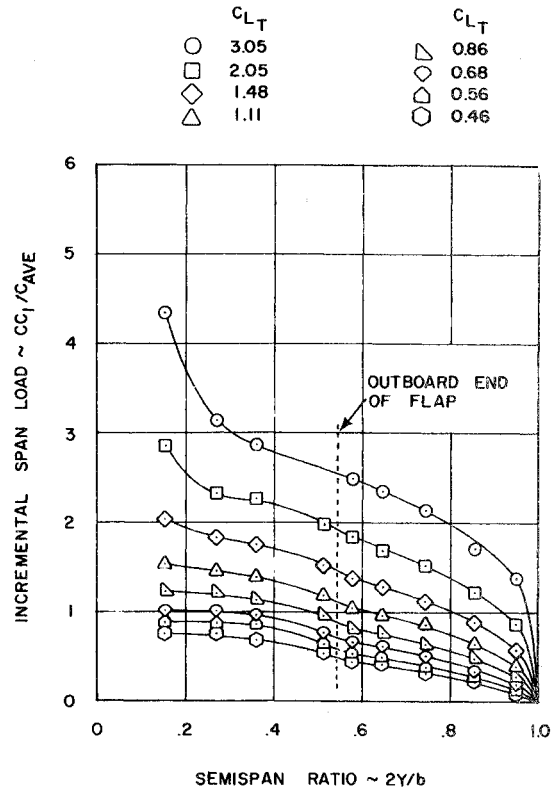

Fig. 3 Span-load distribution, zero flap deflection.

The measurements of the velocity field behind the test aircraft wing were made with a commercially available total-vector hot-film anemometer. The sensor utilized six active film elements, which provided complete definition of the velocity vector. The dimensions of the sensor elements are such that they would fit within an imaginary sphere of 0.3-in. diam. The anemometer was moved throughout the measurement plane by means of a vertical traversing mechanism (VTM), which was mounted to a trolly. The trolly, in turn, was moved along a horizontal boom. The VTM is shown in the mid position in Fig. 2. Thirty-two inches of vertical travel was provided by this mid VTM position. An additional 22 in. of vertical travel was provided by shifting and inverting the VTM on the trolly. For each VTM position, the probe position could be controlled in 1-in. intervals along the 32 in. of vertical travel. The trolly was operated in continuous sweeps over the available 192 in. of lateral travel. During each sweep, the lateral position of the probe was provided by recorded position pulses that were generated at 1-in. intervals along the boom.

The VTM and trolly mechanisms defined a measurement plane inclined at an angle of 6.1° from the vertical when the test aircraft was at zero angle of attack. A coordinate transfer is therefore required to compare data obtained in the measurement plane at a given angle of attack with inviscid flow calculations. Angle-of-attack information provided here is given with respect to the normal to the measurement plane.

For the first test program the lateral boom was mounted to the test aircraft fuselage to provide measurement planes 7.7 and 61.2 in. behind the inboard wing trailing edge (with flaps in the full-up position). These two measurement plane positions are identified as the forward and aft positions in the discussions that follow. The second test program provided measurement plane positions at 5.1, 9.1, and 33.3 in. aft of the inboard wing trailing edge. The first two of these positions provided velocity data that allowed the computation of the longitudinal derivatives of the velocity vector at the forward measurement plane. The 33.3-in. position will be identified hereafter as the mid measurement position. The total vertical travel and the origin of the measurement planes were different

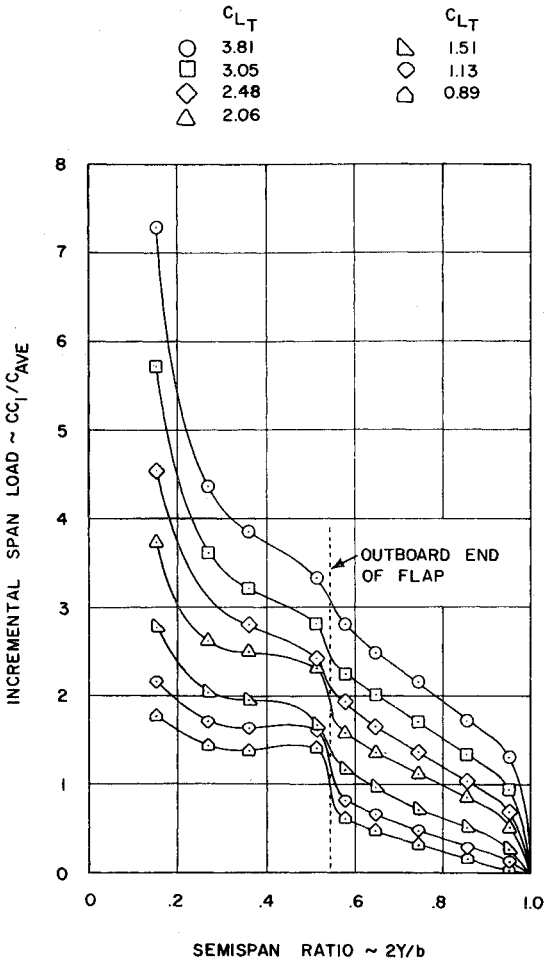

Fig. 4 Span-load distribution, full flap deflection.

for the two test programs, but all data presented in this article are shown with respect to a common measurement plane definition.

All position and instrumentation error corrections were applied to the raw test data. The total-vector anemometer calibration was checked prior to each flight, and suitable calibration voltage was introduced into the system at the beginning and end of each flight. Data reduction was accomplished by digitizing the anemometer data at each of the position pulses on each data sweep. Data noise problems were minimized by averaging ten velocity data samples at each of the position pulses. Application of the anemometer calibration equations provided full velocity component data at each of the 1×1 in. mesh points throughout the measurement plane. The vorticity values were computed for each of the mesh points by evaluating the velocity component derivatives with three-point, collocation-polynomial, finite-difference formulas. The use of five-point difference formulas was studied, but the results showed loss of definition in regions of large vorticity change. No significant improvement in the computed data consistency or apparent accuracy was realized with the five-point formula as compared to the three-point formula. The data for the forward measurement plane, from the first test program, and the mid and aft measurement planes provided data that allowed only the vorticity component normal to the measurement plane to be computed. The two closely spaced forward measurement planes of the second test program allowed calculation of all three components of vorticity.

III. Test Results

The span load distribution data for the two test configurations are given in Figs. 3 and 4 for a range of flight velocities. These data were determined from measured pressure distribution data. The use of the freestream dynamic pressure for computing the section lift coefficients results in the extreme values of loading found in the high dynamic pressure region corresponding to the propeller slipstream. The use of BLC does, of course, make rather large values of section lift coefficient possible over the remaining portions of the wing. The spanwise location of the outboard end of the flap is indicated in these figures. It should be noted that the travel limits of the flap drive system did not allow complete flap retraction, and that about three degrees of flap deflection existed for the configuration labeled "zero flap deflection." The span loading with this minimum flap deflection is, for the most part, quite smooth and does offer the opportunity to obtain full-scale vorticity data for a loading that closely approximates the classical distribution.

Representative vorticity data, determined from the measured velocity data, are shown in Figs. 5-8. These data are presented as contours, within the measurement plane, of constant values of the components of vorticity. The measurement planes are defined in terms of the spanwise y' and upward z' axes where the x' axis is parallel to the downstream normal to the measurement planes. The origin of the measurement plane coordinates is 11 in. below and 12 in. outboard of the inboard end of the flap. A more detailed definition of the relative position of the measurement planes with respect to the aircraft geometry is found in Ref. 6.

The vorticity contours shown in the figures have been normalized according to the following formula

$$\zeta_i^* = \zeta_i / C_L U$$

where ζ_i are the components of mean (i.e., time-averaged) vorticity, U is the test aircraft airspeed, C_L is the test aircraft trimmed lift coefficient, and the asterisk denotes a normalized quantity. The possibility of nondimensionalizing the vorticity through the use of a suitable length scale was considered. This was not done because no single length seemed appropriate for comparison with data for different flap settings or with data for aircraft of different aspect ratios. Although it was not feasible to alter the figures presented in this article, the authors feel future presentations of measured vorticity should include the wingspan as a reference length.

It should also be noted that the test data given here represent the combined results of two separate test programs. Although the results from the two test periods are generally quite consistent, certain differences do appear. The second test program showed some reduction in the peak values of vorticity measured (approximately 10%), and some changes in the location of secondary flow features in the vorticity contours. These differences are noticeable in the figures that show the development of the wake through all three measurement stations. One should therefore take care that the slightly different results from the two programs are not interpreted as longitudinal variations in wake character. No specific source for these differences has been identified, but small variations in the test aircraft configuration between the two test programs could have produced change. Precautions had been taken to prevent such differences, but it is possible that these precautions were inadequate.

The distribution of the three components of vorticity determined for a mean measurement plane location 7.1 in. aft of the wing trailing edge is shown in Fig. 5. These data are presented in terms of contours of constant values of the normalized vorticity component, and represent the zero flap configuration at a trimmed lift coefficient of 1.50, a true velocity of 65.8 mph, and an angle of attack of 18.3°. Except for the spanwise component of vorticity, the flowfield inboard of the outboard edge of the flap is dominated by the BLC system blower exhaust and the propeller slip stream. It is unlikely that much useful information will be found in this inboard region. The presence of a small flap deflection is seen

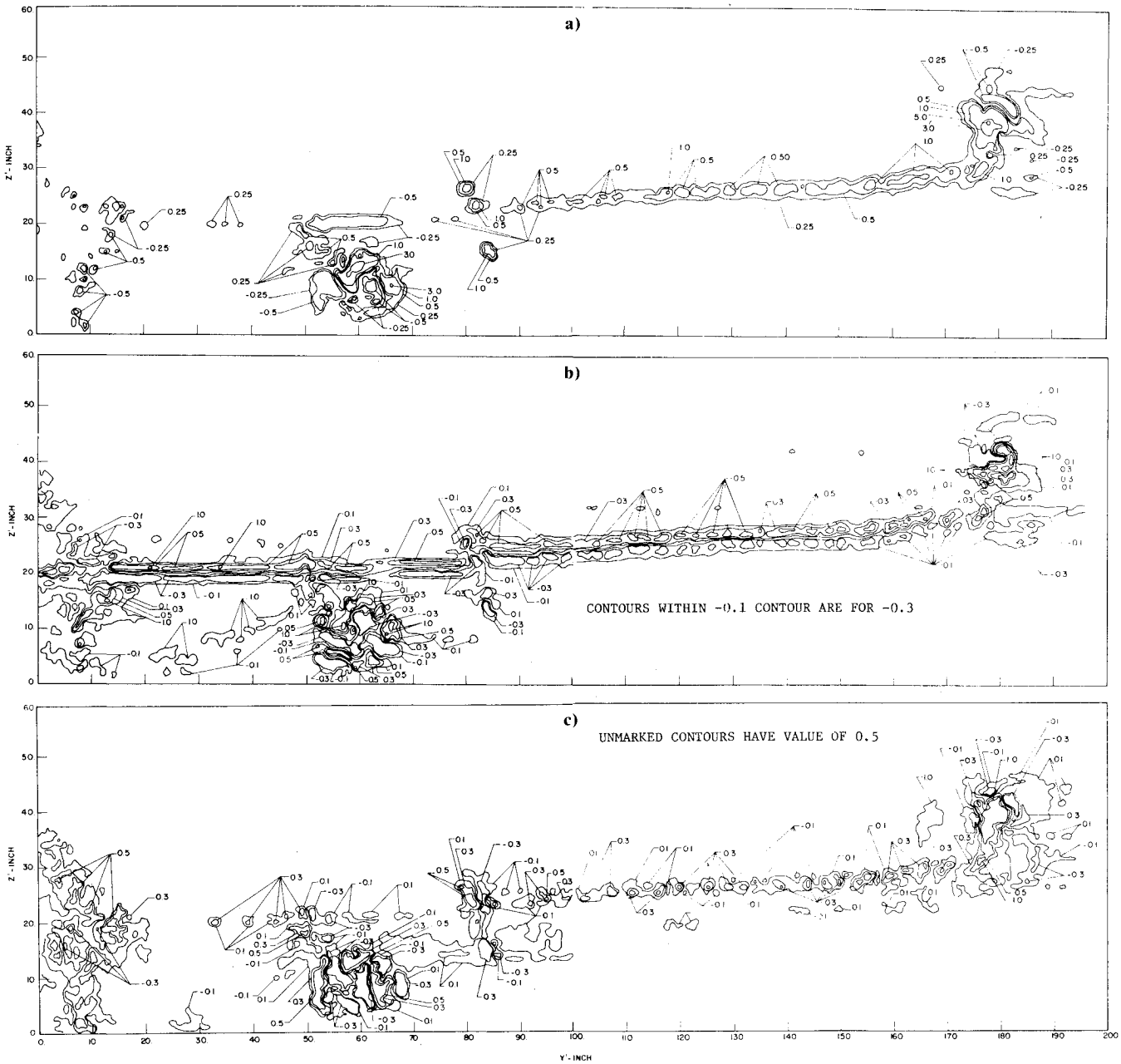

Fig. 5 The three components of vorticity in the forward measurement plane (zero flap deflection, $U = 65.8$ mph, and $C_{L_T} = 1.50$); a) x' component of vorticity, b) y' component of vorticity, and c) z' component of vorticity.

in the resulting step in the spanwise component contour. The role of the boundary-layer development in the formation of the spanwise vorticity component is illustrated by the opposite signs of the spanwise component formed from the upper and lower surfaces of the wing. The vertical array of vorticity (especially the chordwise component) found near $y' = 80$ is probably related to the flap/aileron splitter plate, which can act as a fence with respect to the spanwise component of velocity. Although the chordwise component of vorticity is the dominant component, these data illustrate the need for measuring all the components of vorticity if a complete description of the vorticity field is to be obtained.

Figure 6 represents a comparison of the contours of the chordwise component of vorticity obtained in the three measurement planes for a zero flap configuration. These data represent a nominal trimmed lift coefficient of 1.49, a true airspeed of 65.2 mph, and an angle of attack of 17.9°. The vorticity sheet shed from the wing trailing edge appears to rise when projected onto the measurement plane, but the whole wake system is actually sinking in the downwash velocity field. This will be more clearly demonstrated in the following section where the test results are compared to the inviscid theory calculations. Taking, for example, the portion of the vortex sheet near $y' = 100$, the horizontal projection of the wing trailing edge would be located at vertical positions of 25.9, 34.2, and 43.2 in the forward, mid, and aft measurement planes, respectively. Thus the vortex sheet drops about 10.5 in. over the 53.8 in. between the fore and aft planes. Little curving of the vortex sheet is apparent until the aft measurement plane. Over the longitudinal distance between forward and aft measurement planes, the concentrated vorticity emanating from the region behind the wingtip shows 1 in. of upward travel and 2.5 in. of inboard travel. This concentration of longitudinal vorticity is the first indication of a finite vortex core, with the rest of the sheet beginning to roll around this core as often envisioned in theories of wake formation. This incipient vortex core appears nonaxisymmetric, which is not predicted by inviscid theory, and displays patches of negative vorticity arrayed around its perimeter. These two features always appeared in conjunction with the

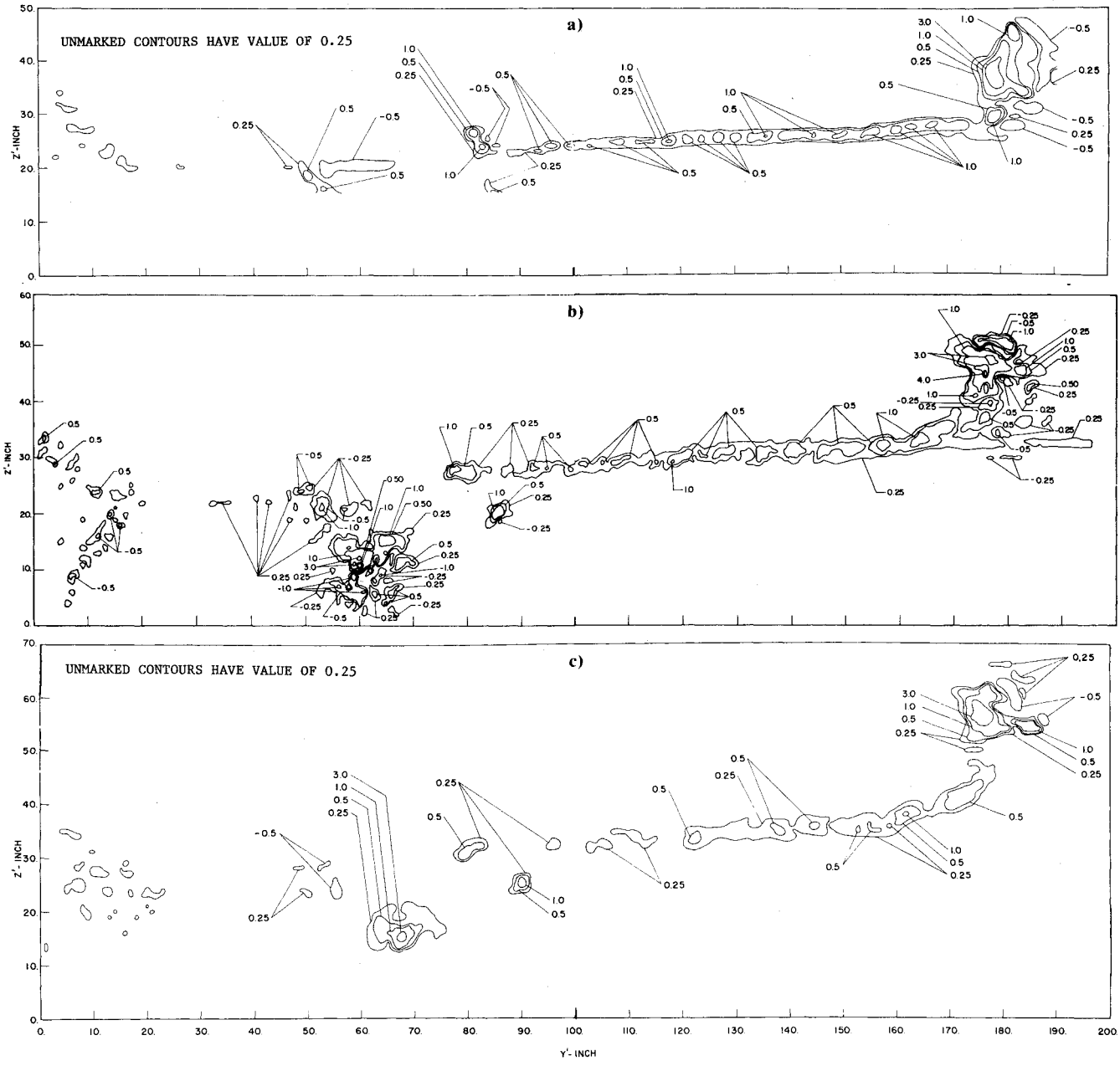

Fig. 6 Normalized x' component of vorticity contours (zero flap deflection, $U = 65.2$ mph, and $C_{L_T} = 1.49$) in the a) forward measurement plane, b) mid measurement plane, and c) aft measurement plane.

early stages of vortex core formation, and are closely associated with this poorly understood process. The diffusion of vorticity during these first stages of wake rollup is also apparent in the figures, and appears quite consistent with the measurements presented by Nielsen and Schwind.[4]

Corresponding contours of longitudinal vorticity for zero flap deflection and a lower value of trimmed lift coefficient are shown in Fig. 7. These data represent a nominal trimmed loft coeficient of 0.87, a true airspeed of 85.6 mph, and an angle of attack of 12.1°. For this case, the vortex sheet (at $y' = 100$) drops 5.5 in. over the longitudinal distance between the fore and aft stations. The concentrated tip vorticity moves upward 2.5 in. and inward 3.5 in. over this same distance. Again, little sheet curvature is apparent until the aft station is reached.

Contours of longitudinal vorticity for the full flap defection configuration at the three measurement planes are given in Fig. 8. This case represents a nominal trimmed lift coefficient of 1.51, a true airspeed of 64.8 mph, and an angle of attack of 9.9°. Here too, the vortex sheet moves downward in the downwash field, and begins to roll up around the tip vortex. In addition, the sheet is also rolling up around the concentration of vorticity immediately behind the outboard edge of the flap. One would suspect that a second vortex core should form at this location, so it is not surprising that the secondary patches of negative vorticity should appear here as well.

Although a large assortment of test data has been provided in the two technical reports produced in conjunction with the research contracts sponsoring this work,[5,6] the data presented here has been chosen to show the primary features of the test results. A full set of three-component velocity data was not considered worth illustrating in detail, but the longitudinal velocity component is especially important in several wake theories. A representative distribution of longitudinal velocity is given in Fig. 9 for the same test aircraft configuration as the case shown in Fig. 7 (zero flap deflection, $C_L = 0.87$). In Fig. 9, all velocity contours have been normalized according to the formula

$$u^*_{x'} = (u_x - U)/C_L U$$

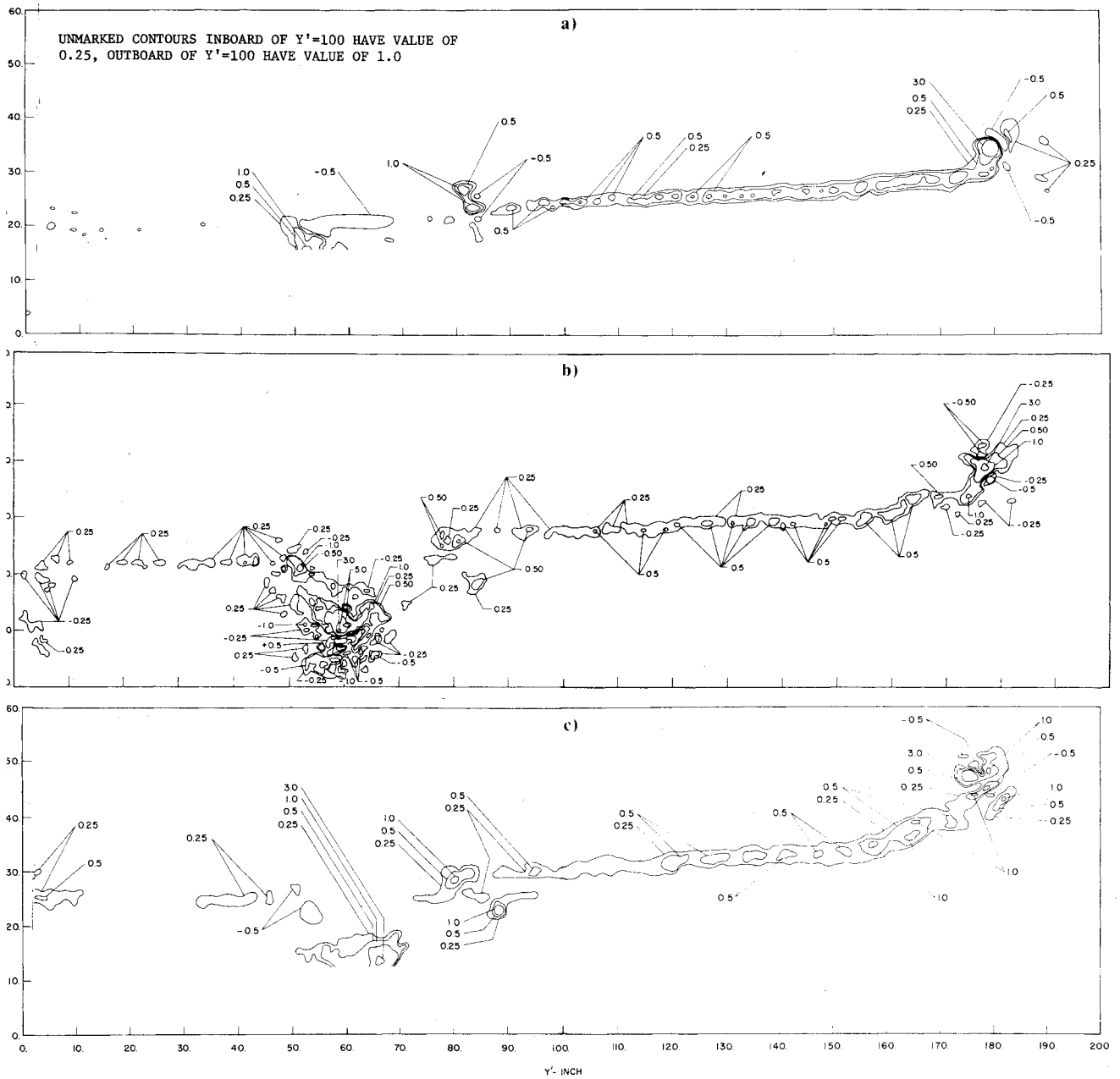

Fig. 7 Normalized x' component of vorticity contours (zero flap deflection, $U = 84.7$ mph, and $C_{L_T} = 0.87$) in the a) forward measurement plane, b) mid measurement plane, and c) aft measurement plane.

In all cases, the formation of what will eventually be a vortex core (including the flap vortex) is associated with an axial velocity excess with maximum values

$$(u_{x'} - U)_{\max} \simeq 0.15 C_L U$$

In a qualitative discussion of vortex formation, Batchelor[7] had speculated that the pressure drop in the center of the growing vortex would produce axial acceleration and a corresponding axisymmetric convergence. The measurements obtained in this experiment appear to confirm Batchelor's theory.

IV. Comparison with Inviscid Theory

The flow dynamics of the near wake are often envisioned as the rolling up of an originally planar sheet of axial vorticity. This process has been modeled numerically by replacing the vortex sheet with an array of finite vortex filaments and allowing the initially flat sheet of elements to move under their collective velocity distributions. Such a theory is obviously inviscid, incompressible, and two-dimensional. This particular method has often been questioned, both in terms of its basic consistency and its numerical stability. For this reason, it was decided to compare the test results given above with the predictions from a finite vortex element calculation of a wake development. The particular version of the method adopted for use here is very similar to the procedure used by Moore,[8] except that the enhanced downwash due to the bound vorticity associated with the lifting surface has also been accounted for. As many as 50 vortex filaments were used per semispan, and the equations were integrated with a fourth-order Runge-Kutta algorithm. The computer program was checked against the published calculations of Moore. It was found that the use of only 20 filaments per semispan gave acceptable accuracy. The test cases were run with the smooth elliptic lift distribution used by Moore. The use of the measured lift distributions of Figs. 3 and 4 greatly aggravated the tendency toward the Helmholtz instabilities in the sheet spiral. These instabilities do not, of course, become important at the extremely small longitudinal distances required for comparison with our test results.

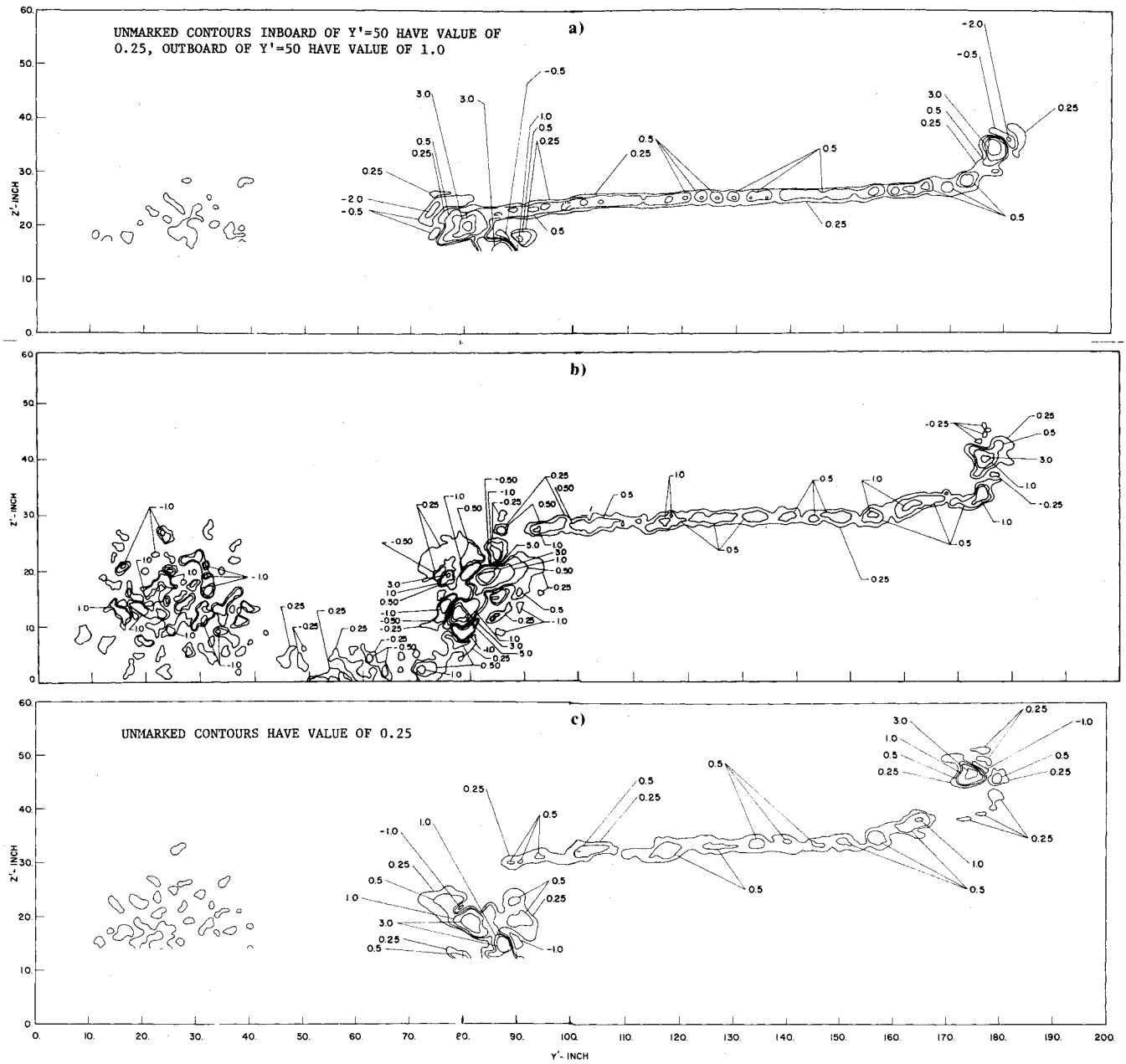

Fig. 8 Normalized x' component of vorticity contours (full flap deflection, $U = 64.8$ mph, and $C_{L_T} = 1.51$) in the a) forward measurement plane, b) mid measurement plane, and c) aft measurement plane.

The inviscid wake theory calculations are compared to one zero flap deflection case in Fig. 10 and to a full flap deflection case in Fig. 11. The agreement, in terms of vortex sheet curvature and tip vortex location, are quite reasonable. It can therefore be concluded that (for relative high aspect ratios, at least) the inviscid theory gives a good estimation of rate of wake rollup. These results also lend justification for the use of such finite element calculations to estimate the effect of wake geometry on airfoil performance. The theory cannot, however, provide any insight into how various viscous or turbulent effects remove the singular behavior associated with the center of the tip vortex in the inviscid approach (see, for example, the discussion by Hall[9]). The secondary features consistently associated with the vorticity concentrations appearing in our test data must be related to these higher order effects.

The generally nonaxisymmetric nature of the tip vortex features that appear in the test data suggest that the stability theory formulated by Lessen et al.[10] might be applicable. These authors found unstable perturbations of the form

$$u' = f(r)\exp\{i(\alpha x + n\phi - \alpha ct)\}$$

where r, ϕ, and x are the usual cylindrical coordinates, α and n are axial and aximuthal wave numbers, c is the complex phase speed, and u' is one of the three components of perturbation velocity. These perturbations were designed to represent traveling waves, whereas the flight-test data given here is steady in time. It had been noted, however, that some of the unstable perturbations had a phase velocity near zero. The eigenfunctions for several such perturbations with near zero phase velocity were calculated, and the distributions of secondary axial vorticity associated with each of them was computed. The results for one such case are illustrated in Fig. 12, where the finite amplitude perturbation has been superimposed on an axisymmetric vortex. The resulting nonsymmetric distribution of positive vorticity and peripheral patches of negative vorticity correspond quite well with the vorticity contours near the concentration of axial vorticity behind the wingtip. The stability theory may thus account for the secondary features that appear when a vortex core is being generated.

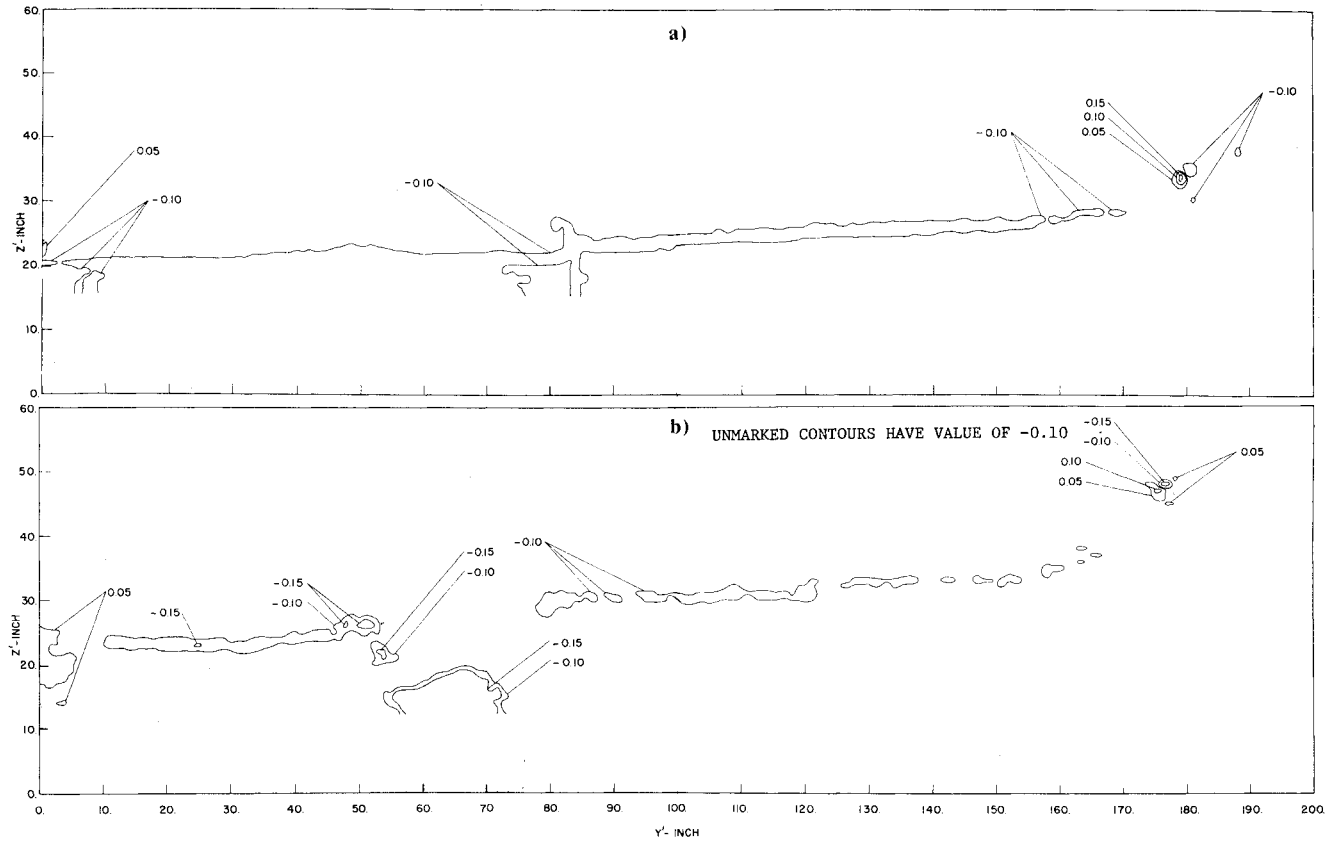

Fig. 9 Normalized longitudinal velocity increment contours for the same flight conditions as Fig. 7 in the a) forward measurement plane and b) aft measurement plane.

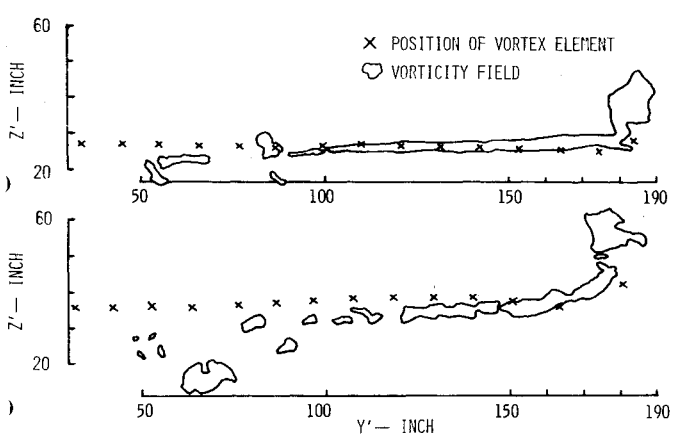

Fig. 10 Finite vortex element calculation superimposed on the vorticity contours of Fig. 6 for the a) forward measurement plane and b) the aft measurement plane (crosses denote location of vortex filaments).

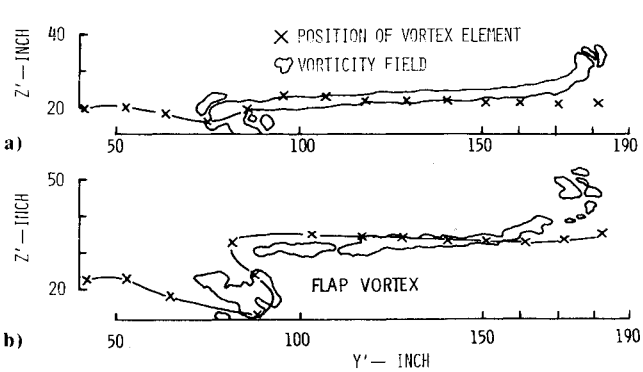

Fig. 11 Finite vortex element calculation superimposed on the vorticity contours of Fig. 8 for the a) forward measurement plane and b) the aft measurement plane.

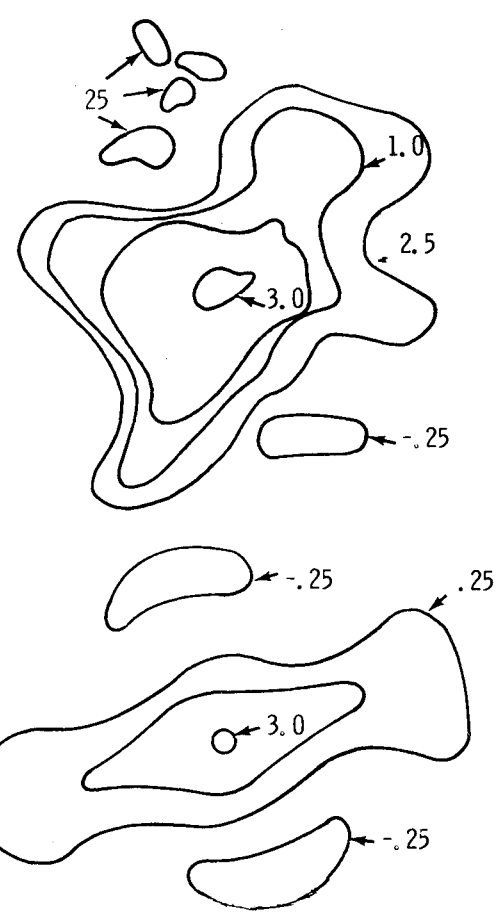

Fig. 12 Comparison of vorticity contours in the tip region of Fig. 8b and a finite amplitude perturbation superimposed on axisymmetric vortex; a) measures vorticity concentration behind tip and b) finite amplitude perturbation.

Acknowledgment

This work was supported by the Air Force Flight Dynamics Laboratory, Wright-Patterson Air Force Base, Ohio, under Contract Number F33615-72-C-1052 and Contract Number F36615-74-C-3066.

References

[1] Olsen, J. H., Goldburg, A., and Rogers, M. (eds), *Aircraft Wake Turbulence and Its Detection*, Plenum Press, New York, 1971.

[2] Chigier, N. A. and Corsiglia, V. P., "Wind Tunnel Studies of Wake Turbulence," *Journal of Aircraft*, Vol. 9, Dec. 1972, p. 820.

[3] McCormick, B. W., Tangler, J. L., and Sherrieb, H. E., "Structure of Trailing Vortices," *Journal of Aircraft*, Vol. 5, May-June 1968, p. 260.

[4] Nielsen, J. N. and Schwind, R. G., "Decay of a Vortex Pair Behind an Aircraft," *Aircraft Wake Turbulence and Its Detection*, edited by J. H. Olsen, A. Goldburg, and M. Rogers, Plenum Press, New York, 1971, p. 413.

[5] Mertaugh, L. J. and Damania, R. B., "An Investigation of the Trailing Vorticity Behind a STOL Aircraft," Air Force Flight Dynamics Laboratory Technical Report, AFFDL-TR-73-138, 1973.

[6] Mertaugh, L. J. and Devarayalu, K., "Further Investigations of the Near Field Trailing Vorticity Behind a STOL Aircraft," Air Force Flight Dynamics Laboratory Technical Report, AFFDL-TR-75-132, 1975.

[7] Batchelor, G. K., "Axial Flow in Trailing Line Vortices," *Journal of Fluid Mechanics*, Vol. 20, Dec. 1964, p. 645.

[8] Moore, D. W., "A Numerical Study of the Roll-Up of a Finite Vortex Sheet," *Journal of Fluid Mechanics*, Vol. 63, April 1974, p. 225.

[9] Hall, M. G., "The Structure of Concentrated Vortex Cores," *Progress in Aeronautical Sciences*, Vol. 7, 1966, p. 61.

[10] Lessen, M., Singh, P. J., and Paillet, F. L., "The Stability of a Trailing Line Vortex, Part 1: Inviscid Case," *Journal of Fluid Mechanics*, Vol. 63, May 1974, p. 753.